α-nucleus optical potential in the double-folding model

Dao T. Khoa
Institute for Nuclear Science & Technique, VAEC, P.O. Box 5T-160, Nghia Do, Hanoi, Vietnam
(Received 19 September 2000; published 22 February 2001)

The double-folding formalism for the α-nucleus optical potential is revised to study the exchange effects and density dependence of the effective nucleon-nucleon (NN) interaction in detail. A realistic density dependent M3Y interaction, based on the G-matrix elements of the Paris NN potential, has been used in the folding calculation. The local approximation for the nonlocal one-body density matrix in the calculation of the exchange potential was tested by using the harmonic oscillator representation of the nonlocal density matrices of the α-particle and target nucleus. The inclusion of a realistic density dependence into the effective NN interaction was shown to be *vital* for a correct description of the refractive α-nucleus scattering data. A high sensitivity of the density distributions of the α-particle and target nucleus to the shape of the α-nucleus potential was found, which can be used in the folding analysis to test various density models for the α-particle and target as well as to choose the most realistic approximation for the overlap density in the dinuclear system. Our results also stress the importance of α-nucleus scattering experiment in the nuclear structure study.

DOI: 10.1103/PhysRevC.63.034007 PACS number(s): 21.30.Fe, 24.10.Ht, 24.50.+g, 25.55.Ci

I. INTRODUCTION

During the past two decades, the double-folding model [1] has been widely used to generate the real parts of both the α-nucleus and heavy-ion (HI) optical potentials. It is straightforward to see that folding model generates the first-order term in the expression for the microscopic optical potential that is derived from Feshbach's theory of nuclear reactions [2]. The success of this approach in describing the observed elastic scattering of many systems suggests that the first-order term of the microscopic optical potential is indeed the dominant part of the real HI optical potential [3].

The basic inputs for a folding calculation are the nuclear densities of the colliding nuclei and the effective nucleon-nucleon (NN) interaction. A popular choice for the effective NN interaction has been one of the M3Y interactions which were designed to reproduce the G-matrix elements of the Reid [4] and Paris [5] NN potentials in an oscillator basis. These density *independent* M3Y interactions have been used with some success in folding model calculations of the HI optical potential at relatively low energies [1], where the data are sensitive to the potential only at the surface. However, in cases of refractive nuclear scattering, characterized by the observation of ''rainbow'' features (see Refs. [6–11]), the scattering is sensitive to the optical potential over a wider radial domain and the simple M3Y-type interaction failed to give a good description of the data. This has motivated the inclusion of an explicit density dependence into the original M3Y interactions [12], to account for the reduction in the attractive strength of the effective NN interaction that occurs as the density of the nuclear medium increases.

A Hartree-Fock study of nuclear matter (NM) [13,14] has also shown that, as expected [15], the original density *independent* M3Y interaction [4,5] failed to saturate cold NM, leading to collapse. Therefore, several parametrizations of the density dependence (DD) for the M3Y interaction were introduced [13,14,16] in order to reproduce the observed NM saturation density and binding energy. Although different versions of the DD give, by design, the same saturation values, they do result in different values of the nuclear incompressibility K. These density dependences of the M3Y interaction have been carefully tested in the folding analysis of refractive α-nucleus and light HI elastic scattering [13,14,16,17], and one was able to conclude from these studies that K values ranging from 240 to 270 MeV are the most appropriate for the cold nuclear matter [16] (an important conclusion for the nuclear equation of state).

The main features of the new version of the folding model [16,18,19] are the inclusion of a realistic DD into the effective NN interaction and the explicit treatment of the exchange potential using a realistic local approximation. In general, the calculation of the exchange potential is quite complicated due to its nonlocality. An accurate local approximation can be obtained for the exchange potential by treating the relative motion locally as a plane wave, similar to the prescription developed for the nucleon-nucleus optical potential [20,21]. However, the evaluation of the *localized* exchange potential still contains a self-consistency problem and involves an explicit (six-dimensional) integration over the nonlocal density matrices of the two colliding nuclei. Ismail *et al.* [22] have recently studied the accuracy of the local approximation for the one-body density matrix (DM) in the folding model using the wave function based on harmonic oscillator model. They have shown that the numerical error of the local approximation for the one-body DM could be up to 20%, but did not check this in any optical model (OM) analysis of elastic nucleus-nucleus scattering. A more accurate study of the single-nucleon exchange in the double-folding model by Soubbotin and Viñas [23] has shown that the local approximation for the one-body DM used in the folding model is quite appropriate if a realistic expression is used for the kinetic energy density. But they have not checked either the discussed effect in the OM analysis of elastic data.

In the light of these results, we find it necessary to consider the problem in more detail. The best testing ground for our purpose is the *refractive* α-nucleus elastic scattering, where the data were proven to be very sensitive to the real

optical potential at small distances. We also show in the present study how the introduction of the DD into the M3Y interaction affects the folding potential and compare this with the effect caused by different treatments of the exchange term.

II. THE DOUBLE-FOLDING MODEL

The details of the double-folding formalism are given in Ref. [19] and we only recall briefly its main features. In general, the projectile-target (real) optical potential can be evaluated as a Hartree-Fock-type potential of the dinuclear system

$$V=\sum_{i\in a,j\in A}[\langle ij|v_D|ij\rangle+\langle ij|v_{EX}|ji\rangle]=V_D+V_{EX}, \quad (1)$$

where the nuclear interaction V is a sum of the effective NN interactions v_{ij} between nucleon i in the projectile a and nucleon j in the target A. The antisymmetrization of the dinuclear system is done by taking into account the so-called single-nucleon knock-on exchange effects (the interchange of nucleons i and j).

The direct term is local (provided that the NN interaction itself is local), and can be written in terms of the one-body spatial densities,

$$V_D(E,\boldsymbol{R})=\int \rho_a(\boldsymbol{r}_a)\rho_A(\boldsymbol{r}_A)v_D(\rho,E,s)d^3r_a d^3r_A,$$

$$\boldsymbol{s}=\boldsymbol{r}_A-\boldsymbol{r}_a+\boldsymbol{R}, \quad (2)$$

where $\rho_a(\boldsymbol{r}_a)\equiv\rho_a(\boldsymbol{r}_a,\boldsymbol{r}_a)$ is the diagonal part of the nonlocal (one-body) density matrix for the projectile, and similarly for $\rho_A(\boldsymbol{r}_A)$ for the target nucleus.

The exchange term is, in general, nonlocal. However, an accurate local approximation can be obtained by treating the relative motion locally as a plane wave [20,21]

$$V_{EX}(E,\boldsymbol{R})=\int \rho_a(\boldsymbol{r}_a,\boldsymbol{r}_a+\boldsymbol{s})\rho_A(\boldsymbol{r}_A,\boldsymbol{r}_A-\boldsymbol{s})v_{EX}(\rho,E,s)$$

$$\times\exp\left(\frac{i\boldsymbol{K}(E,\boldsymbol{R})\boldsymbol{s}}{M}\right)d^3r_a d^3r_A. \quad (3)$$

$\boldsymbol{K}(E,\boldsymbol{R})$ is the local momentum of relative motion determined as

$$K^2(E,\boldsymbol{R})=\frac{2\mu}{\hbar^2}[E_{\rm c.m.}-V(E,\boldsymbol{R})-V_C(\boldsymbol{R})], \quad (4)$$

μ is the reduced mass, $M=aA/(a+A)$ with a and A the mass numbers of the projectile and target, respectively. In the calculation of the local momentum $V(E,\boldsymbol{R})=V_D(E_\alpha,\boldsymbol{R})+V_{EX}(E_\alpha,\boldsymbol{R})$ and $V_C(\boldsymbol{R})$ are the total nuclear and Coulomb potentials, respectively.

Local approximation for the one-body density matrix

Even the evaluation of the exchange potential in the localized form (3) is complicated: it contains a self-consistency problem because $K(E,R)$ depends upon the potential $V(E,R)$ itself, and involves the integration over the nonlocal (one-body) density matrices of the colliding nuclei. In general, the nuclear densities $\rho_{a(A)}(r)$ are taken either from an accurate nuclear structure model or directly from the electron scattering data, and the calculation of the exchange potential (3) can be done [16,18] by using a realistic approximation for the nonlocal DM [20,24]

$$\rho(\boldsymbol{r},\boldsymbol{r}+\boldsymbol{s})\simeq\rho\left(\boldsymbol{r}+\frac{\boldsymbol{s}}{2}\right)\hat{j}_1\left(k_F\left(\boldsymbol{r}+\frac{\boldsymbol{s}}{2}\right)s\right), \quad (5)$$

with

$$\hat{j}_1(x)=3j_1(x)/x=3(\sin x-x\cos x)/x^3. \quad (6)$$

To accelerate the convergence of the DM expansion, Campi and Bouyssy (CB) [24] have suggested to choose, for a spherically symmetric ground state density, the local Fermi momentum $k_F(r)$ in the following form:

$$k_F(r)=\left\{\frac{5}{3\rho(r)}\left[\tau(r)-\frac{1}{4}\nabla^2\rho(r)\right]\right\}^{1/2}. \quad (7)$$

Assuming the CB prescription, we choose further the extended Thomas-Fermi approximation for the kinetic energy density $\tau(r)$, and the local Fermi momentum is obtained as

$$k_F(r)=\left\{\left[\frac{3}{2}\pi^2\rho(r)\right]^{2/3}+\frac{5C_S[\nabla\rho(r)]^2}{3\rho^2(r)}+\frac{5\nabla^2\rho(r)}{36\rho(r)}\right\}^{1/2}, \quad (8)$$

where C_S is the strength of the so-called Weizsäcker term representing the surface contribution to τ. For a finite fermionic system, the commonly accepted value of the Weizsäcker term [25] is $C_S=1/36$, denoted hereafter as CB1 approximation. It was also suggested [26] that in a region of small density or high $\nabla\rho$ (like the nuclear surface) the Weizsäcker correction term to the kinetic energy density should be enhanced and have a strength of $C_S=1/4$, denoted hereafter as CB2 approximation. In our previous folding calculations [16–18] we have used the CB2 approximation which generally gives a slightly better OM fit to the data. The recent studies [22,23] of the DM expansion have shown, however, that the CB1 approximation gives a more correct local expression for the DM. We will discuss this aspect here in more detail by comparing results given by the CB local ap-

TABLE I. Harmonic oscillator parameters [see Eqs. (12) and (15)] for the ground state densities of the α particle, ^{12}C, and ^{16}O with the corresponding rms radii.

Nucleus	Version	b (fm)	rms (fm)	Reference	rms[a] (fm)	rms[b] (fm)
^{4}He	A	1.4044	1.7200	Ref. [23]	1.47 ± 0.02	1.58 ± 0.04
	B	1.2658	1.5503	this work		
	C	1.1932	1.4613	Ref. [1]		
^{12}C		1.5840	2.3316	this work	2.33 ± 0.01	2.35 ± 0.02
^{16}O		1.7410	2.6115	this work	2.61 ± 0.01	

[a]Empirical rms radius given by the experimental charge density from elastic electron scattering data [41] unfolded with the finite-size proton distribution.

[b]Empirical rms radius given by the Glauber model analysis [42,43] of the experimental interaction cross section.

proximation with the ''exact'' results in cases where a simple harmonic oscillator model is appropriate for the DM.

Assuming the local CB approximation (5) and using the energy and density dependent exchange interaction $v_{EX}(\rho,E,s)$ given below in Sec. III, one easily obtains the self-consistent and local exchange potential V_{EX} as

$$V_{EX}(E,R)=4\pi\int_0^\infty v_{EX}(\rho,E,s)j_0(K(E,R)s/M)s^2ds \times\int f_a(r,s)f_A(|\boldsymbol{r}-\boldsymbol{R}|,s)d^3r, \tag{9}$$

where

$$f_{a(A)}(r,s)=\rho_{a(A)}(r)\hat{j}_1(k_{F_{a(A)}}(r)s). \tag{10}$$

The exchange potential (9) can then be evaluated by an iterative procedure which converges very fast.

Exact treatment of the one-body density matrix using harmonic oscillator representation

The simple harmonic oscillator (h.o.) model was already used by Campi and Bouyssy [24] to treat explicitly the nonlocality of the DM for the justification of the local approximation (5)–(7). In the same way, it is possible to explicitly evaluate the exchange part of the folding potential (3) using the h.o. model for the DM. One should keep in mind, however, that the h.o. model is a simple approach which cannot give the correct description of the nuclear surface and asymptotic tail of the density distribution. Therefore, we consider here only systems of strongly bound nuclei like α particle or ^{12}C (for which the use of h.o. model is reasonable).

α particle is a unique case where a simple Gaussian can reproduce very well its ground state density [1]. Assuming 4 nucleons to occupy the lowest $s\frac{1}{2}$ h.o. shell in ^{4}He, one obtains exactly the nonlocal ground state DM for the α particle as

$$\rho_\alpha(\boldsymbol{r},\boldsymbol{r}+\boldsymbol{s})=\rho_\alpha\left(\left|\boldsymbol{r}+\frac{\boldsymbol{s}}{2}\right|\right)\exp\left(-\frac{s^2}{4b_\alpha^2}\right), \tag{11}$$

where

$$\rho_\alpha(r)\equiv\rho_\alpha(r,r)=\frac{4}{\pi^{3/2}b_\alpha^3}\exp\left(-\frac{r^2}{b_\alpha^2}\right). \tag{12}$$

If one takes the h.o. parameter $b_\alpha=1.1932$ fm (version C in Table I) then the density (12) is exactly the Gaussian form for the α density adopted in Ref. [1], which has a rms radius of 1.461 fm (quite close to the empirical value of 1.47 ±0.02 fm).

In recent years, many interesting data have been measured for systems involving p-shell nuclei like ^{12}C and ^{16}O. The h.o. form has already been used in the past [27] for the densities of these nuclei in the folding model calculation, and it is expected to be reasonable if the h.o. parameter is chosen to reproduce the empirical value of rms radius. With 12 nucleons in ^{12}C fully occupying the lowest $s\frac{1}{2}$ and $p\frac{3}{2}$ h.o. shells, $\rho(\boldsymbol{r},\boldsymbol{r}+\boldsymbol{s})$ is in general a nonlocal function which also depends upon the relative orientation between the two vectors $\boldsymbol{r}$ and $\boldsymbol{s}$. However, the effect due to different orientations between $\boldsymbol{r}$ and $\boldsymbol{s}$ is negligible compared to the DM value itself [22,24] (see numerical ''error bars'' in Fig. 1 of Ref. [24]), and one can represent the ground state DM for ^{12}C explicitly as

$$\rho(\boldsymbol{r},\boldsymbol{r}+\boldsymbol{s})=\frac{4}{\pi^{3/2}b^3}\left(1+\frac{4|\boldsymbol{r}+\boldsymbol{s}|r}{3b^2}\right)\exp\left(-\frac{s^2}{4b^2}-\frac{\left|\boldsymbol{r}+\frac{\boldsymbol{s}}{2}\right|^2}{b^2}\right). \tag{13}$$

Assuming the lowest $s\frac{1}{2}$, $p\frac{3}{2}$, and $p\frac{1}{2}$ h.o. shells fully occupied by 16 nucleons in ^{16}O, the ground state DM for this nucleus can be represented in the same way as

$$\rho(\boldsymbol{r},\boldsymbol{r}+\boldsymbol{s})=\frac{4}{\pi^{3/2}b^3}\left(1+\frac{2|\boldsymbol{r}+\boldsymbol{s}|r}{b^2}\right)\exp\left(-\frac{s^2}{4b^2}-\frac{\left|\boldsymbol{r}+\frac{\boldsymbol{s}}{2}\right|^2}{b^2}\right). \tag{14}$$

The ground state density of ^{12}C or ^{16}O is evaluated as diagonal part of the density matrix (13) or (14)

TABLE II. Parameters for the Fermi model [see Eq. (18)] of the ground state density distributions for ^{12}C, ^{16}O, ^{58}Ni, and ^{90}Zr with the corresponding rms radii.

Nucleus	Version	ρ_0 (fm^{-3})	c (fm)	a (fm)	rms (fm)	Reference	rms[a] (fm)
^{12}C	I	0.207	2.1545	0.425	2.298	Ref. [28]	2.33±0.01
	II	0.194	2.214	0.425	2.332	this work	
^{16}O	I	0.181	2.525	0.450	2.574	Ref. [28]	2.61±0.01
	II	0.168	2.600	0.450	2.618	Ref. [46]	
^{58}Ni		0.176	4.080	0.515	3.695	Ref. [19]	3.68±0.01
^{90}Zr		0.165	4.900	0.515	4.251	Ref. [28]	4.20±0.01

[a]Empirical rms radius given by the experimental charge density from elastic electron scattering data [41] unfolded with the finite-size proton distribution.

$$\rho(r)\equiv\rho(r,r)=\frac{4}{\pi^{3/2}b^3}\left(1+\frac{F_p\,r^2}{b^2}\right)\exp\left(-\frac{r^2}{b^2}\right), \quad (15)$$

where $F_p=4/3$ and 2 for ^{12}C and ^{16}O, respectively. The chosen h.o. parameters b for these nuclei are given in Table I.

Using Eqs. (12) and (13), it can be shown that the exchange potential for α-particle incident on a p-shell (target) nucleus is still evaluated by Eq. (9) but using, instead of the CB local approximation (10), the exact density profiles in the following forms:

$$f_\alpha(r,s)=\rho_\alpha(r)\exp\left(-\frac{s^2}{4b_\alpha^2}\right), \quad (16)$$

and

$$f_A(r,s)=\frac{4}{\pi^{3/2}b^3}\left[1+\frac{F_p}{b^2}\left(r^2-\frac{s^2}{4}\right)\right]\exp\left(-\frac{s^2}{4b^2}-\frac{r^2}{b^2}\right). \quad (17)$$

We note that Eqs. (13)–(15) were derived explicitly for ^{12}C and ^{16}O. In case the $p\frac{3}{2}$ or $p\frac{1}{2}$ shell is not fully occupied, one should normalize the $p\frac{3}{2}$ or $p\frac{1}{2}$ component of the h.o. wave function to the neutron or proton numbers in this shell before adding it to the $s\frac{1}{2}$ part to obtain the full wave function. As a result, one obtains the same expressions (15) and (17) for the ground state density and density profile $f_A(r,s)$, respectively, but with a different F_p number. Similarly, for a system involving two p-shell nuclei like ^{12}C+^{12}C, ^{16}O+^{12}C , and ^{16}O+^{16}O , where the ground state DM's can be approximately described by the h.o. model, the exchange potential can be evaluated by Eq. (9) but using the exact expression (17) for the density profiles $f_{a(A)}(r,s)$ instead of the CB local approximation (10).

In this case, one can test the validity of the CB local approximation for the DM by comparing the exchange potential obtained using approximation (10) with that obtained using the exact expressions (16) and (17). The most accurate approximation has to be used in general case, when the nuclear density cannot be described by the h.o. model. In the present work, besides the h.o. representations (12) and (15), the nuclear densities are also taken, as in our previous folding calculations [16,18], in the two-parameter Fermi form

$$\rho(r)=\rho_0/[1+\exp((r-c)/a)]. \quad (18)$$

Parameters in Eq. (18) were chosen to reproduce correctly the nuclear rms radii as suggested by electron scattering data or by the shell model calculations [1,28,29]. The density parameters of nuclei studied in this work are given in Table II.

III. EFFECTIVE NN INTERACTION

The effective *NN* interaction and the adjustments of its density dependent parameters to reproduce the saturation properties of nuclear matter have been described in detail elsewhere [13,14,16]. In general, the interaction is assumed to have a separable form

$$v_{D(EX)}(\rho,s)=F(\rho)v_{D(EX)}(s), \quad (19)$$

where v_D and v_{EX} are the direct and exchange terms, respectively, derived from the M3Y interactions [4,5], and s is the internucleon separation; ρ is the density of the surrounding nuclear medium in which the two nucleons are embedded. The radial shape of the M3Y-Paris interaction [5] used in the present folding calculation, are given in terms of three Yukawas. Its explicit form can be found, e.g., in Refs. [16,19]. The density dependence $F(\rho)$ is taken in the CDM3Y6 form which was introduced in Ref. [16]. Its parameters were chosen to reproduce the NM saturation properties and a value of nuclear matter incompressibility $K=252$ MeV (see Table I in Ref. [16]).

The overlap density ρ in $F(\rho)$ is usually taken to be the sum of the projectile and target densities. In the case of exchange potential (3), the overlap density ρ is the total density at the midpoint between the two nucleons being exchanged,

$$\rho=\rho_a\left(\boldsymbol{r}_a+\frac{\boldsymbol{s}}{2}\right)+\rho_A\left(\boldsymbol{r}_A-\frac{\boldsymbol{s}}{2}\right). \quad (20)$$

In addition to the energy dependence of the folded potential arising from the exchange term, it was found necessary to include an ''intrinsic'' energy dependence into the M3Y interaction, in order to reproduce the empirical energy depen-

dence of the nucleon-nucleus optical potential [13,30]. This additional energy dependence was incorporated in a separable form so that Eq. (19) becomes

$$v_{D(EX)}(\rho,E,s)=g(E)F(\rho)v_{D(EX)}(s) =(1-0.003E_{\rm lab}/a)F(\rho)v_{D(EX)}(s), \quad (21)$$

where $E_{\rm lab}/a$ is the energy per nucleon (in MeV).

As discussed in Sec. II, the main effect of antisymmetrization under exchange of nucleons between the two nuclei that is included in the folding model is the single nucleon knock-on exchange in which the two nucleons interacting via $v_{EX}(s)$ are interchanged. To avoid explicit treatment of the nonlocality in the calculation of the exchange potential, a simple zero-range exchange (ZE) pseudopotential is still widely used instead of the finite-range exchange, which replaces $v_{EX}(s)\rightarrow\hat{J}(E)\,\delta(\mathbf{s})$ in Eq. (3). The magnitude of $\hat{J}(E)$ has been determined empirically [31] by comparing with the exact results for proton scattering from various targets, at energies up to 80 MeV. Explicit $\hat{J}(E)$ value for the M3Y-Paris interaction can be found, e.g., in Ref. [3].

IV. FOLDING ANALYSIS OF THE ELASTIC ALPHA-NUCLEUS SCATTERING

It is now well established that elastic α-nucleus scattering at intermediate energies is strongly refractive. In this case, the absorption is quite weak and the measured elastic scattering cross sections were shown to be sensitive to the *real* α-nucleus potential not only at the surface but also at shorter distances. Consequently, one can use such data to test different models for the α-nucleus optical potential. The smaller the distance the stronger the overlap of the projectile and target, and hence the density dependence of the effective *NN* interaction plays a crucial role. The folding model has been used successfully to analyze refractive α-nucleus and light HI elastic scattering [14,17,16], to infer the most realistic DD for the M3Y interaction.

The real optical potential $V(E,R)$ obtained in Sec. II must be supplemented by an imaginary potential which account for the absorption into nonelastic channels. In some cases it was found sufficient to simply treat the effective *NN* interaction as having a complex strength so that the real and imaginary optical potentias have the same radial shape. However, the *weak* absorption found in the refractive α-nucleus [32] and light HI [3,33] systems requires that the imaginary potential should have a different shape (the ratio of the imaginary to the real potential tends to peak at the surface and becomes relatively weak in the interior). Therefore, it is common to use the folding model to calculate the real potential and to use a Woods-Saxon (WS) form for the imaginary potential. Thus, the local optical potential $U(E,R)$ in our OM analysis of the elastic α-nucleus scattering is

$$U(E,R)=V_C(R)+N_V[V_D(E,R)+V_{EX}(E,R)]+iW(R), \quad (22)$$

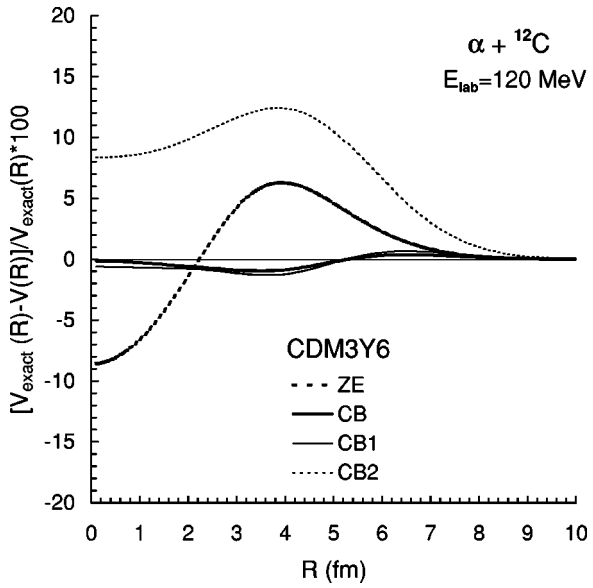

FIG. 1. Numerical accuracy (in %) of the folding potentials for $\alpha+{}^{12}$C system at $E_{\rm lab}=120$ MeV obtained with the h.o. model for the α and ^{12}C densities, using different local approximations (see caption and footnote in Table III) for the nonlocal one-body DM. Results were obtained using the density dependent CDM3Y6 interaction.

where the imaginary WS part of the optical potential is given by

$$W(R)=-\frac{W}{1+\exp((R-R_W)/a_W)}. \quad (23)$$

The renormalization factor N_V, together with the WS parameters are adjusted in each case for the best fit to the elastic data. All the OM analyses were made using the code PTOLEMY [34]. The inputs for masses and energies in the folding calculation as well as in the OM analysis were taken as given by the relativistically corrected kinematics [35].

$\alpha+{}^{12}$C system

^{12}C target is a well-known ''refractive'' target for different light projectiles, ranging from α particle [36] to ^{12}C [8,9] and ^{16}O [11,37]. From numerous $\alpha+{}^{12}$C elastic data we have selected the data at $E_{\rm lab}=104$ MeV [39], 120, 145 and 172.5 MeV [40], which have been shown to be strongly refractive, with an overwhelming domination of the far-side scattering at large angles [36].

We have chosen for the folding analysis of elastic $\alpha+{}^{12}$C data version C of the α density (see Table I), which has been used so far in most of the folding analyses of α-nucleus scattering. For ^{12}C target, the h.o. form (13) and (16) of the DM was used. In Fig. 1 we have plotted the relative difference (in %) of the folding potentials for $\alpha+{}^{12}$C system at $E_{\rm lab}=120$ MeV, calculated using different versions of the CB local approximation (10) for the DM, from the exact results obtained using Eqs. (16) and (17). One can see that the most accurate is the CB1 local approximation [see Eq. (8) and the discussion after]. The error caused

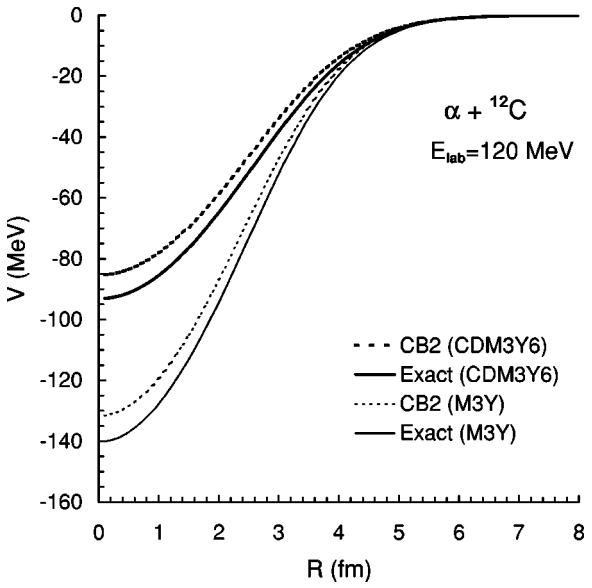

FIG. 2. Radial shape of the folding potentials for $\alpha+{}^{12}$C system at $E_{\rm lab}=120$ MeV obtained with the h.o. model for the α and ^{12}C densities, using the CB2 local approximation (dotted curves) and exact treatment (solid curves) of the nonlocal one-body DM. Results obtained with density *independent* M3Y interaction and density *dependent* CDM3Y6 interaction are plotted, respectively, by thin and thick curves.

by the use of the CB1 approximation for ^{12}C target or for both the α particle and ^{12}C target is only around 1% which is much less than other uncertainties of the folding model. Both the CB2 approximation and the simple zero-range exchange prescription can lead to an error of up to 15%. Thus, they are less accurate compared to the CB1 approximation.

Concerning the introduction of a realistic DD into the effective M3Y interaction, from the results plotted in Fig. 2 one finds immediately that the difference in the folding potentials calculated with or without a DD in the M3Y interaction is much more substantial compared to the errors caused by using different CB local approximations for the DM. The folding potentials calculated using the density *independent* interaction are much deeper compared to those calculated using the same local approximations and density *dependent* interaction. The relative difference amounts up to 30–40 % at small radii. This is the reason why the folding model using the density *independent* effective *NN* interaction usually fails to describe the refractive α-nucleus elastic scattering data. The inclusion of a realistic DD into the original M3Y interaction, necessary for the correct description of the nuclear matter saturation properties [13,14,16], substantially reduces the strength of the folding potential at small distances. Our folding results obtained for the incident α energies ranging from 40 to 172.5 MeV have shown about the same effects as discussed here for the energy of 120 MeV. Thus, the effects shown in Figs. 1 and 2 are practically energy independent.

We now show how the effects discussed above for the folding potential can affect the calculated elastic cross section. Since a difference in the *real* optical potential can be well compensated by some change of the *imaginary* potential, one has to consider, for this purpose, refractive (elastic) data which are strongly sensitive to the real optical potential. We have chosen the elastic $\alpha+{}^{12}$C data at 120 and 172.5 MeV for our detailed folding analysis and the obtained OM parameters are given in Table III. We found that the difference caused by different local approximations for the DM's of the α particle and ^{12}C target shown in Fig. 1 can lead to a slight difference (well within the uncertainty of the measured data) in the calculated elastic cross sections at large angles, provided that N_V factor and WS parameters of the imaginary potential are chosen by the least χ^2 fit to the data. The main effect that can be traced is the enhancement of the renormalization factor for the folding potential. Namely, the best-fit N_V factor found with the CB2 approximation is about 12–14 % larger than that found with the exact treatment of nonlocal DM or with the CB1 approximation (Table III). About the same difference is found in potentials at distances around 4 fm (Fig. 1), and the considered elastic data are probably sensitive to the real optical potential at such small distances. The CB2 local approximation is less accurate compared to the CB1 approximation and gives a N_V value deviating stronger from unity. We note that with the inclusion of a realistic DD into the M3Y interaction, all versions of the $\alpha+{}^{12}$C folding potential (if renormalized properly) describe the data reasonably well.

The folding potentials calculated with the density *independent* M3Y interaction are much deeper than those obtained with the density *dependent* interaction, and such a difference (up to 30–40 % as shown in Fig. 2) cannot be eliminated by simply renormalizing the real folded potentials. Even with the exact treatment of the nonlocal DM in the exchange term, the folding potential gives a much worse fit to the data if there is no DD included into the effective M3Y interaction (see Figs. 3 and 4). The OM fits with the ''density independent'' folding potentials tend to give N_V values substantially smaller (by 40–50 %) as well as the parameters of the imaginary WS potential deviating strongly from those obtained with ''density dependent'' potentials. Such a failure of the density independent M3Y interaction in the description of the refractive data has been discussed in the past, and here we show that this effect is much stronger than the uncertainty from different CB local approximations.

The folding results discussed so far were obtained with the h.o. model for the ^{12}C density. Since the simple h.o. model usually cannot give a correct description of the asymptotic tail of the density distribution, it is of interest to make the same analysis using a more flexible form for ^{12}C density. For this purpose, we have used two versions of the Fermi model (18) for ^{12}C density. Parameters of version I (see Table II), which has been widely used in the previous folding analyses for systems involving ^{12}C, were adjusted [28] to give the shape and rms radius close to those given by the shell model calculation. Its rms radius of 2.298 fm is slightly smaller than the empirical value of 2.33 fm deduced from elastic electron scattering [41]. The empirical matter radius of ^{12}C might be somewhat larger (2.35 ± 0.02 fm) if one adopts the result given by the Glauber model analysis [42,43] of the experimental interaction cross section. Therefore, we have chosen the h.o. parameter b and the new Fermi parameters (version II) for ^{12}C such that they reproduce in

TABLE III. Optical potential parameters [see Eqs. (22) and (23)] used in the folding analysis of the elastic $\alpha+{}^{12}$C data at $E_{\rm lab}=104$, 120, 145, and 172.5 MeV. The folding potentials were obtained using version C of the α density and three choices for the ^{12}C density (Tables I and II). Different approximations for the nonlocal DM are abbreviated as follows: Exact=exact treatment of nonlocal DM's for both α and ^{12}C using the h.o. model; CB=exact treatment of the nonlocal DM for α and CB1 local approximation for ^{12}C; CB1=CB1 local approximation for both α and ^{12}C; CB2=CB2 local approximation for both α and ^{12}C. χ^2 values are per datum, and were obtained with experimental errors.

$E_{\rm lab}$ (MeV)	^{12}C dens.	DM	DD[a]	N_V	$\langle r^2\rangle_V^{1/2}$ (fm)	J_V (MeV fm^3)	W (MeV)	R_W (fm)	a_W (fm)	σ_R (mb)	χ^2
104	har.osc.	Exact	Yes	1.136	3.392	329.8	17.93	3.891	0.556	785.5	9.7
	Fermi II	CB	Yes	1.126	3.398	326.5	17.76	3.866	0.572	785.9	10.5
	Fermi I	CB	Yes	1.119	3.382	319.0	17.72	3.817	0.593	784.6	12.1
120	har.osc.	ZE[b]	No	0.631	3.206	238.8	24.35	2.561	1.034	841.8	24.0
	har.osc.	Exact	No	0.707	3.267	263.2	20.33	3.231	0.840	808.3	19.5
	har.osc.	ZE[b]	Yes	1.138	3.368	311.7	23.09	3.430	0.708	800.3	5.6
	har.osc.	CB2	Yes	1.307	3.398	327.6	21.31	3.711	0.618	793.5	5.0
	har.osc.	CB1	Yes	1.150	3.394	326.0	20.79	3.773	0.596	789.7	6.7
120	har.osc.	Exact	Yes	1.166	3.397	327.8	20.92	3.772	0.595	790.2	6.1
	Fermi II	CB	Yes	1.157	3.403	324.7	20.74	3.742	0.611	791.0	6.3
	Fermi I	CB	Yes	1.143	3.386	315.5	20.90	3.659	0.643	790.8	7.7
145	har.osc.	Exact	Yes	1.159	3.404	309.8	19.35	3.858	0.599	769.5	2.2
	Fermi II	CB	Yes	1.150	3.410	306.9	18.65	3.862	0.618	774.3	2.3
	Fermi I	CB	Yes	1.146	3.394	300.8	17.87	3.868	0.636	777.1	2.7
172.5	har.osc.	ZE[b]	No	0.627	3.221	217.7	12.67	3.821	0.816	742.0	12.3
	har.osc.	Exact	No	0.730	3.281	245.7	14.18	3.911	0.716	743.1	8.3
	har.osc.	ZE[b]	Yes	1.064	3.383	267.1	21.21	3.351	0.795	758.5	3.6
	har.osc.	CB2	Yes	1.297	3.417	295.6	21.81	3.770	0.558	714.4	3.2
	har.osc.	CB1	Yes	1.145	3.411	292.3	20.75	3.808	0.568	721.6	3.4
172.5	har.osc.	Exact	Yes	1.162	3.413	294.1	21.02	3.814	0.557	718.6	3.3
	Fermi II	CB	Yes	1.137	3.417	287.0	20.50	3.718	0.626	731.8	3.5
	Fermi I	CB	Yes	1.121	3.402	278.5	19.48	3.673	0.680	743.5	3.9

[a]Density dependence of the *NN* interaction: ''Yes'' when the CDM3Y6 version for $F(\rho)$ is used with the M3Y interaction; ''No'' when no density dependence is used, i.e., $F(\rho)=1$.

[b]Simple zero-range approximation (see discussion in Sec. III) is used for the exchange potential.

both models a rms radius of 2.332 fm. For both versions of the Fermi density, the folding calculation was performed with the exact treatment of the nonlocal DM for α and the CB1 local approximation for the DM of ^{12}C target. Results of the OM analyses of the elastic $\alpha+{}^{12}$C data at four energies are given in Table III and shown in Fig. 5. As one can see, all three versions of ^{12}C density give about the same fit to the data, with some difference seen at largest angles, especially at 145 and 172.5 MeV. Since the h.o. and Fermi II densities have the same rms radius, the corresponding folded potentials also have about the same rms radius, N_V factor and volume integral per interacting nucleon pair J_V (Table III). The folding potential obtained with version I of the Fermi model for ^{12}C density has, as expected, smaller rms and J_V values, and it gives a slightly worse χ^2 fit to the data. This shows that the rms radius of the chosen density distribution is very important in the folding model.

$\alpha+{}^{16}$O system

^{16}O nucleus, due to its double-closed shell structure, has been proven to be also a strong ''refractive'' target, which has been studied extensively in elastic ^{16}O+^{12}C [11,37] and ^{16}O+^{16}O scattering [17,38] at different energies. Some of available elastic $\alpha+{}^{16}$O data show quite a strong refractive structure, and we have considered elastic $\alpha+{}^{16}$O data at $E_{\rm lab}=54.1$ MeV [44], 80.7 MeV [45], and 104 MeV [39]. These data cover a wide angular range and have a broad shoulderlike maximum, typical for the nuclear rainbow.

The errors caused by two versions of the CB local approximation (10) for the nonlocal DM's in the folding calculation were found about the same for the $\alpha+{}^{16}$O system as shown in Fig. 1 for $\alpha+{}^{12}$C. The most accurate is the CB1 approximation which has the error of only around 1%. The difference in the folding potentials calculated with or without a DD in the M3Y interaction was also found much more substantial compared to that caused by the two CB local approximations. The use of the density dependent interaction is crucial for a correct description of the data over the whole angular range (see Fig. 6).

To test the ^{16}O density, we have analyzed the elastic $\alpha+{}^{16}$O scattering data at $E_{\rm lab}=54.1$, 80.7, and 104 MeV using the CDM3Y6 folding potential obtained with the h.o. model

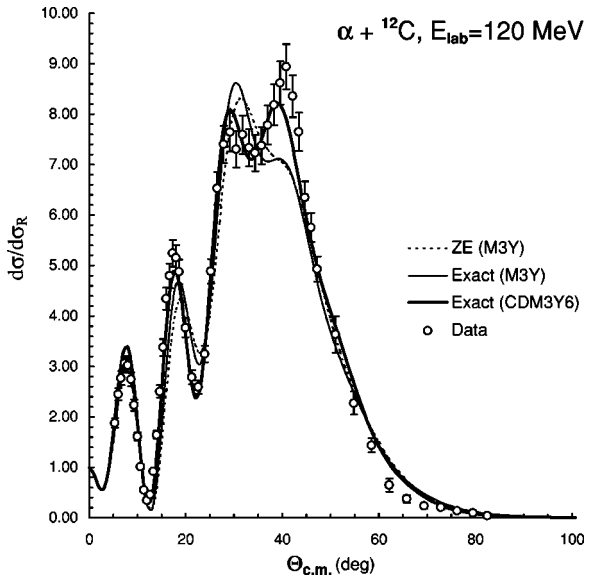

FIG. 3. Elastic $\alpha+{}^{12}$C scattering data at $E_{\rm lab}=120$ MeV plotted in linear scale, in comparison with the OM fits given by the folding potentials obtained with the h.o. model for the α and ^{12}C densities, using density *independent* M3Y interaction and density *dependent* CDM3Y6 interaction. The corresponding OM parameters are given in Table III.

(Table I) and two versions of the Fermi model (Table II) for the ^{16}O density. The conclusion is that all three versions of the ^{16}O density are appropriate for the folding calculation. Version II of the Fermi model [46] and the h.o. form for the ^{16}O density have rms values very close to the empirical radius of 2.61 ± 0.01 fm, and they give almost the same folding potential (see N_V and other OM parameters in Table IV).

A consistent test of different choices for the α density is also important for the folding analyses of the elastic and, especially, *inelastic* α-nucleus scattering [19], where the accurate input for the α density is necessary because the same factor N_V, as obtained from the OM analysis, is to be used further (in the DWBA calculation) to renormalize the transition folding potential. We have performed the folding analysis of the same $\alpha+{}^{16}$O scattering data using three different choices for the α density (Table I). Version A of the α density has the h.o. parameter ($b_\alpha=1.4044$ fm) taken from Ref. [23], which gives a rms radius of 1.72 fm (larger than the empirical value by about 0.25 fm). This b_α value was obtained as variational parameter in a self-consistent Hartree-Fock calculation which gives the α binding energy of 28.24 MeV, quite close to the experimental value. Version C of the α density is exactly the Gaussian form adopted in Ref. [1], which has a rms radius close to that deduced from the elastic electron scattering data. Recently, the Glauber model has been often used to deduce the nuclear radius from the analysis of the experimental interaction cross sections, and the rms radius obtained for ^{4}He is around 1.58 fm [42,43]. We have chosen, therefore, also a h.o. parameter $b_\alpha=1.2658$ fm (version B) which gives a rms radius of 1.55 fm, close to the result of the Glauber analysis. Radial

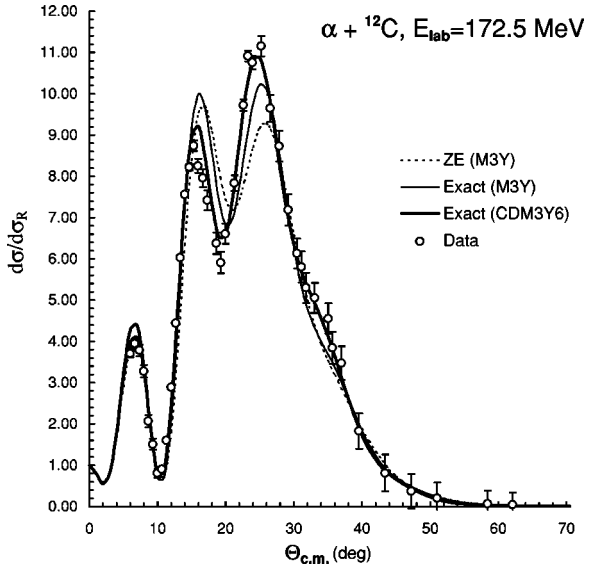

FIG. 4. The same as in Fig. 3, but for $\alpha+{}^{12}$C system at $E_{\rm lab}=172.5$ MeV.

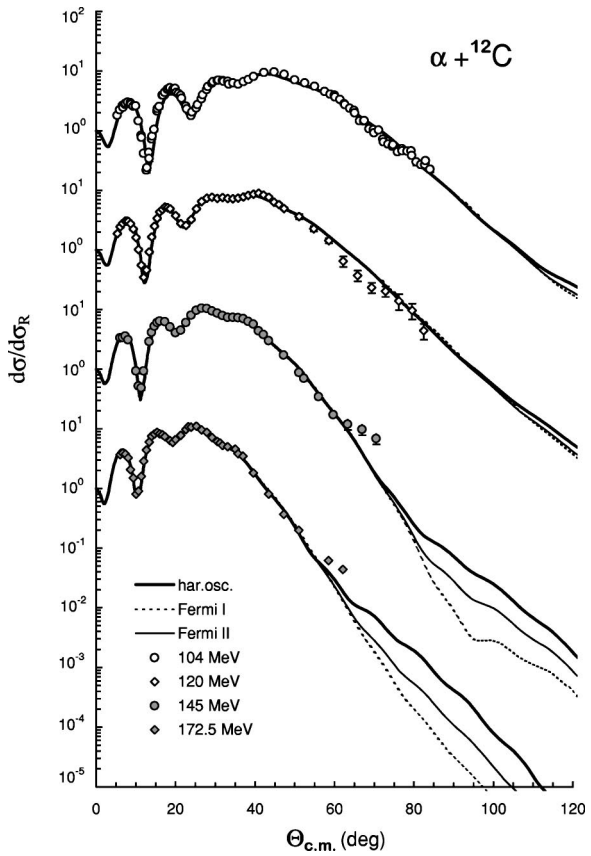

FIG. 5. Elastic $\alpha+{}^{12}$C scattering data at $E_{\rm lab}=104$, 120, 145, and 172.5 MeV in comparison with the OM fits given by the folding potentials obtained with the h.o. model and two versions of the Fermi model for the ^{12}C density, using the density dependent CDM3Y6 interaction. The nonlocal DM of the α particle was treated exactly in all cases using version C of the α density. The nonlocal DM of the ^{12}C target was treated exactly with the h.o. density, and in the CB1 approximation with the Fermi density. The corresponding OM parameters are given in Table III.

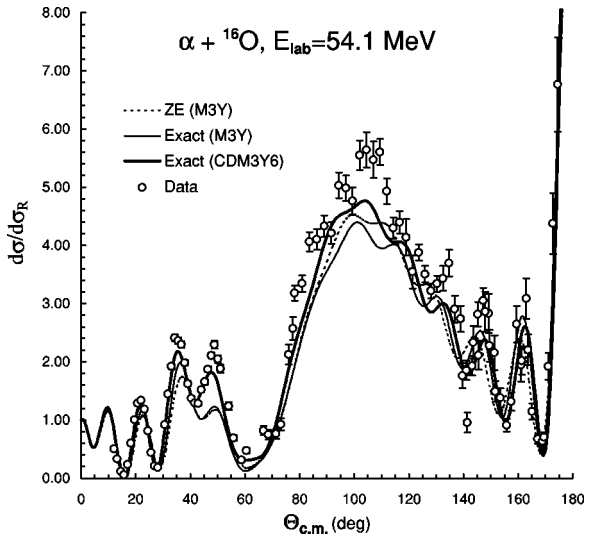

FIG. 6. Elastic $\alpha+{}^{16}$O scattering data at $E_{\rm lab}=54.1$ MeV plotted in linear scale, in comparison with the OM fits given by the folding potentials obtained with the h.o. model for the α and ^{16}O densities, using density *independent* M3Y interaction and density *dependent* CDM3Y6 interaction. The corresponding OM parameters are given in Table IV.

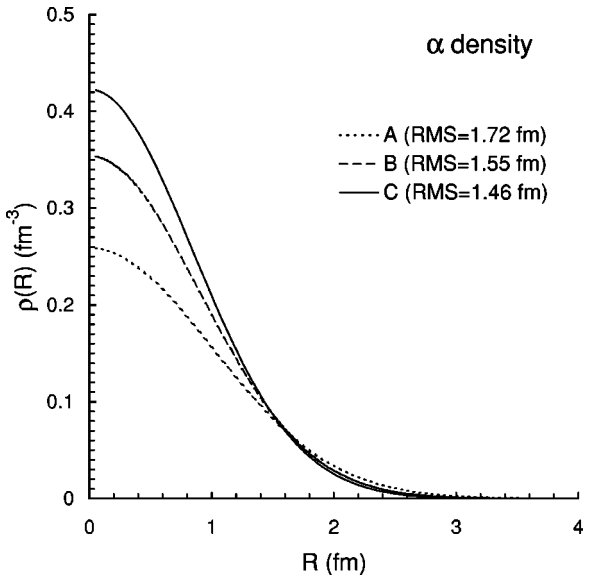

FIG. 7. Radial shape of three versions of the h.o. model for the α ground state density used in the present folding calculation. See details in Table I.

shape of the three h.o. versions for the α density is shown in Fig. 7, and the corresponding folding potentials for the $\alpha+{}^{16}$O system at 54.1 MeV are shown in Fig. 8. As the difference between the densities is more substantial in the center of the α particle, the difference in the potentials is largest at small distances. From our experience, this effect might best be seen in the calculated cross sections at large angles, in the refractive region.

We found that the folding potential obtained using version A of the α density gives a worse fit to the data compared to other two cases (see χ^2 values given by these potentials in Table III). The difference between results given by versions B and C is rather small and well within the experimental errors. Since the difference is significant in the calculated cross section at large angles, we have further tested the α density in a *restricted* OM fit to the data points at forward angles only (see Fig. 9). The data at forward angles (in diffractive region) are sensitive to the α-nucleus potential at the

TABLE IV. Optical potential parameters [see Eqs. (22) and (23)] used in the folding analysis of the elastic $\alpha+{}^{16}$O data at $E_{\rm lab}=54.1$, 80.7, and 104 MeV. The folding potentials were obtained using different choices for the α and ^{16}O densities (Tables I and II) and the density dependent CDM3Y6 interaction. The approximations for the nonlocal DM are denoted in the same way as in Table III. χ^2 values are per datum, and were obtained with uniform 10% errors.

$E_{\rm lab}$ (MeV)	α dens.	^{16}O dens.	DM	N_V	$\langle r^2\rangle_V^{1/2}$ (fm)	J_V (MeV fm^3)	W (MeV)	R_W (fm)	a_W (fm)	σ_R (mb)	χ^2
54.1	C	Fermi I	CB	1.140	3.576	368.3	12.99	4.084	0.682	1004	6.8
	C	Fermi II	CB	1.141	3.601	375.7	12.76	4.147	0.667	1010	6.4
	C	har.osc.	Exact	1.137	3.591	375.4	12.79	4.152	0.665	1011	6.4
	B	har.osc.	Exact	1.082	3.620	383.5	12.62	4.192	0.667	1025	6.1
	A	har.osc.	Exact	1.032	3.687	402.9	12.11	4.298	0.684	1069	7.1
80.7	C	Fermi I	CB	1.131	3.582	346.0	16.09	4.219	0.604	949.6	1.0
	C	Fermi II	CB	1.137	3.607	354.2	15.83	4.287	0.583	954.0	1.0
	C	har.osc.	Exact	1.138	3.597	355.3	15.79	4.309	0.574	954.2	1.1
	B	har.osc.	Exact	1.085	3.626	363.4	15.55	4.356	0.572	966.5	1.7
	A	har.osc.	Exact	1.032	3.692	380.5	15.14	4.416	0.616	1019	4.4
104	C	Fermi I	CB	1.095	3.587	319.3	19.52	4.054	0.687	965.3	1.8
	C	Fermi II	CB	1.096	3.612	325.4	19.71	4.072	0.682	971.8	1.6
	C	har.osc.	Exact	1.096	3.602	326.1	20.01	4.067	0.679	972.0	1.8
	B	har.osc.	Exact	1.038	3.631	331.2	20.35	4.050	0.691	984.3	2.1
	A	har.osc.	Exact	0.966	3.696	339.1	21.34	3.962	0.742	1021	5.7

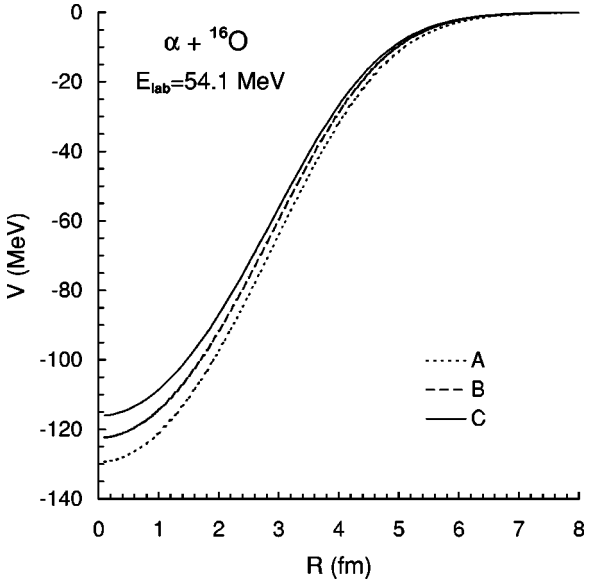

FIG. 8. Radial shape of the folding potentials for the $\alpha+{}^{16}\mathrm{O}$ system at $E_{\mathrm{lab}}=54.1$ MeV obtained with the density dependent CDM3Y6 interaction and the h.o. model for the α and $^{16}\mathrm{O}$ densities. The nonlocal one-body DM's of the two nuclei were treated exactly in all cases. Different versions of the α density are taken from Table I.

surface, and thus are necessary for the determination of the renormalization factor N_V. After factor N_V and WS parameters of the imaginary potential were fixed from such a restricted OM fit, the measured elastic cross section at large angles (in refractive region) is a subject to the predictive power of the folding potential. One can see from Fig. 9 that the folding potential obtained with version C of the α density is evidently the best choice for the real optical potential. Version A gives a folding potential somewhat deeper (see Fig. 8), which fails to describe the data at large angles. Version B seems to give a better shape for the potential but still unable to describe the large angle data points at 80.7 MeV, where the rainbow maximum is most pronounced. These results show again that the correct rms radius is very crucial in choosing the density distribution. They also indicate that the rms radius deduced from the elastic electron scattering data for the α particle seems to be more accurate than that deduced from the Glauber model analysis of the interaction cross sections.

From the results presented here for $\alpha+{}^{12}\mathrm{C}$ and $\alpha+{}^{16}\mathrm{O}$ systems we also conclude that the chosen h.o. form and version II of the Fermi model for the $^{12}\mathrm{C}$ and $^{16}\mathrm{O}$ densities, which have the rms values close to the empirical data [41], are quite appropriate for the folding model calculation. The folding parameters obtained should be a helpful guide in the prediction of the α-nucleus optical potential for the elastic scattering of loosely bound p-shell nuclei on α target.

$\alpha+{}^{58}$Ni system

For a completeness of the study, we present further results of the folding analysis of elastic α scattering data for heavier targets. We have considered the elastic $\alpha+{}^{58}\mathrm{Ni}$ scattering

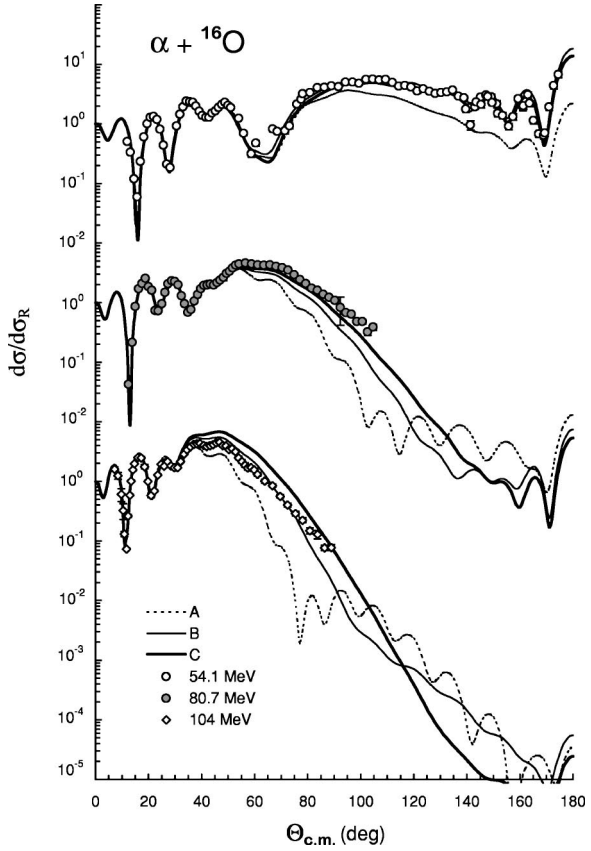

FIG. 9. Elastic $\alpha+{}^{16}\mathrm{O}$ scattering data at $E_{\mathrm{lab}}=54.1$, 80.7, and 104 MeV in comparison with *restricted* OM fits given by the folding potentials obtained with three versions of the α density and h.o. model for the $^{16}\mathrm{O}$ density, using the density dependent CDM3Y6 interaction. The OM fit was performed for data points at $\theta_{\mathrm{c.m.}} \leqslant 58.7°$, $34.8°$, and $29.6°$ for $E_{\mathrm{lab}}=54.1$, 80.7, and 104 MeV, respectively.

data at $E_{\mathrm{lab}}=82$ MeV [47], 104 MeV [48], 139 MeV [6], and 172.5 MeV [49]. These elastic $\alpha+{}^{58}\mathrm{Ni}$ scattering data are among the best experimental evidences for nuclear rainbow scattering. For example, the elastic $\alpha+{}^{58}\mathrm{Ni}$ data at 139 MeV were the first that led one to the importance of density dependence in the folding model analysis (see, e.g., Ref. [12] and references therein). The data sets for $E_{\mathrm{lab}}=104$, 139, and 172.5 MeV have been analyzed earlier [16] using the density dependent CDM3Y6 interaction. However, the CB2 local approximation was used in Ref. [16] and it is necessary to have the folding analysis done using the more accurate CB1 local approximation.

Results of the folding analysis using three versions of the α density are compared with the data in Fig. 10, and the corresponding OM parameters are given in Table V. The folding potentials used in this analysis differ from each other in about the same way as shown in Fig. 8 for the $\alpha+{}^{16}\mathrm{O}$ system. Judging by the χ^2 values given in Table V, one finds that the cross section obtained with version A of the α density gives a worse fit to the data. On the logarithmic plot the cross-section difference between the three cases seems to be still within the uncertainty of the measured data, except for the data at 104 MeV, where the potential based on version A

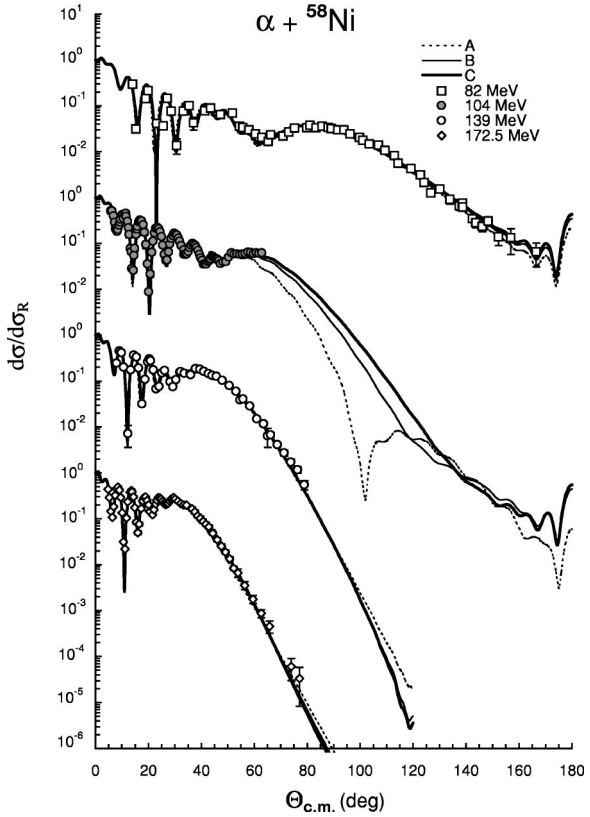

FIG. 10. Elastic $\alpha+{}^{58}$Ni scattering data at $E_{\rm lab}=82$, 104, 139, and 172.5 MeV in comparison with the OM fits given by the folding potentials obtained with three versions of the α density and Fermi form for the ^{58}Ni density, using the density dependent CDM3Y6 interaction. The nonlocal one-body DM of the α particle was treated exactly and that of the ^{58}Ni target was treated in the CB1 approximation. The corresponding OM parameters are given in Table V.

of the α density fails to describe the last data points and generates a broad oscillation at large angles, where the rainbow tail of the elastic cross section should fall down smoothly. Compared to the folding results obtained for these cases using version C of the α density and the CB2 local approximation [16], the present folding results (using version C of the α density and the CB1 local approximation) give about the same fit to the data, but have a renormalization factor $N_V\approx 1.06$ which is by about 15% smaller than that obtained in Ref. [16] (see Table V of this work and Table II of Ref. [16]). We note that the optimum N_V values obtained so far in the folding analyses of the elastic α-nucleus scattering (using both finite-range or zero-range exchange interactions) are greater than unity and lie between 1.2 and 1.3 [12,14,16,50], and no satisfactory explanation could have been given. By using the most accurate local approximation for the nonlocal DM in the calculation of the exchange potential, the best-fit N_V values (see also results obtained for the $\alpha+{}^{90}$Zr system presented below) become smaller by about 15% and closer to unity.

To test the α density, we have also performed a *restricted* OM fit to the elastic $\alpha+{}^{58}$Ni data at 139 and 172.5 MeV, in the same manner as done above in the $\alpha+{}^{16}$O case (see Fig. 11). With the renormalization factor N_V and WS parameters of the imaginary potential fixed by the restricted OM fit, all three potentials describe very well the data points at forward angles. However, the large-angle data can only be correctly described with version C of the α density, and this result confirms that version C is the most realistic for the α density. Note that the difference in rms radius between versions B and C is only about 0.1 fm (Table I), but it can show up in the calculated cross section if the chosen incident energy is high enough for a clear observation of refractive features (around 25 MeV/nucleon).

It is also noteworthy that our folding analysis of the elastic $\alpha+{}^{12}$C, $\alpha+{}^{16}$O, and $\alpha+{}^{58}$Ni data gives the total reac-

TABLE V. Optical potential parameters [see Eqs. (22) and (23)] used in the folding analysis of the elastic $\alpha+{}^{58}$Ni data at $E_{\rm lab}=82$, 104, 139, and 172.5 MeV. The folding potentials were obtained with three versions of the α density and Fermi form for the ^{58}Ni density (Tables I and II), using the density dependent CDM3Y6 interaction. The nonlocality of the DM was treated exactly for α and in the CB1 local approximation for ^{58}Ni. χ^2 values are per datum, and were obtained with experimental errors.

$E_{\rm lab}$ (MeV)	α dens.	N_V	$\langle r^2\rangle_V^{1/2}$ (fm)	J_V (MeV fm^3)	W (MeV)	R_W (fm)	a_W (fm)	σ_R (mb)	χ^2
82	A	0.948	4.646	320.8	17.57	6.223	0.650	1716	27.7
	B	1.000	4.593	307.5	18.26	6.098	0.650	1669	21.2
	C	1.053	4.571	301.8	18.51	6.049	0.650	1650	18.8
104	A	0.913	4.646	295.2	21.32	6.218	0.561	1647	22.5
	B	1.002	4.594	294.7	20.16	6.164	0.598	1648	10.8
	C	1.073	4.572	294.2	20.10	6.117	0.619	1650	12.2
139	A	0.912	4.648	275.0	22.12	5.759	0.833	1784	18.5
	B	0.989	4.597	271.2	21.59	5.832	0.754	1699	5.1
	C	1.053	4.575	269.2	21.61	5.838	0.730	1670	2.4
172.5	A	0.892	4.650	251.8	31.17	5.265	0.815	1650	10.3
	B	0.985	4.600	252.9	27.17	5.433	0.807	1655	4.3
	C	1.056	4.579	252.9	25.98	5.513	0.789	1645	4.0

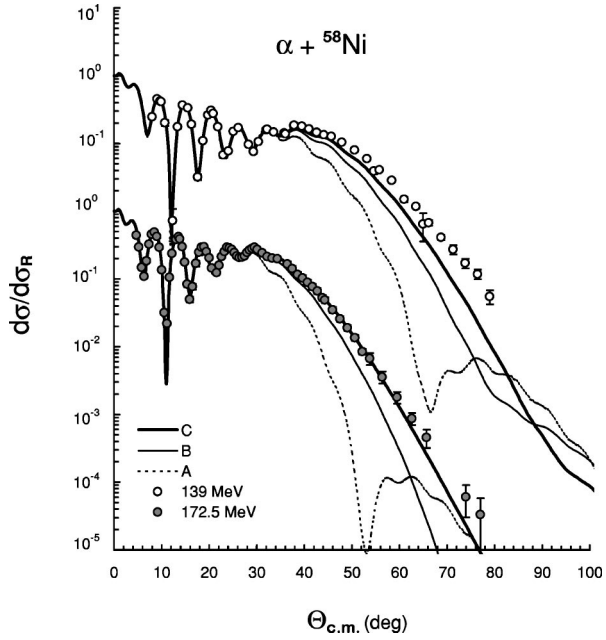

FIG. 11. Elastic $\alpha+{}^{58}$Ni scattering data at $E_{\rm lab}=139$ and 172.5 MeV in comparison with *restricted* OM fits given by the folding potentials obtained with three versions of the α density and Fermi form for the ^{58}Ni density, using the density dependent CDM3Y6 interaction. The OM fit was performed for data points at $\theta_{\rm c.m.} \leqslant 36^\circ$ and 29.5° for $E_{\rm lab}=139$ and 172.5 MeV, respectively.

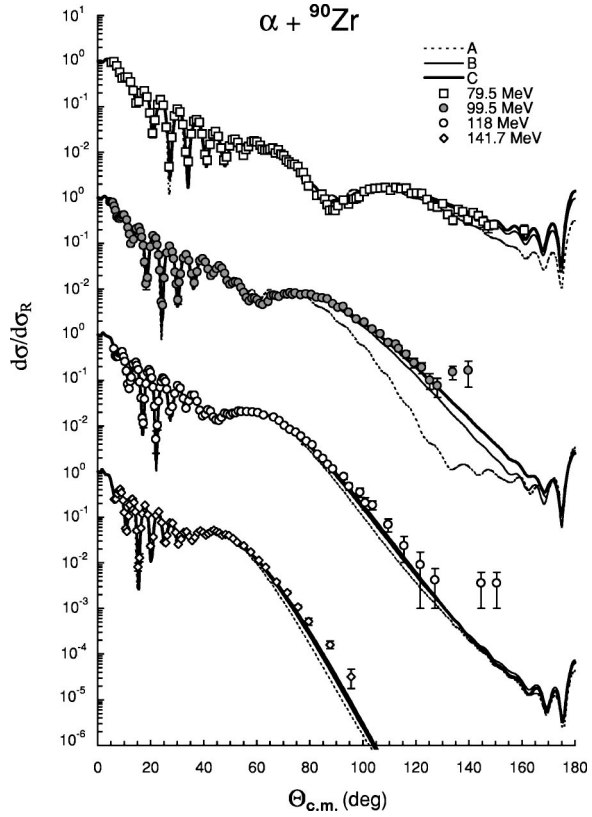

FIG. 12. Elastic $\alpha+{}^{90}$Zr scattering data at $E_{\rm lab}=79.5$, 99.5, 118, and 141.7 MeV in comparison with the OM fits given by the folding potentials obtained with three versions of the α density and Fermi form for the ^{90}Zr density, using the density dependent CDM3Y6 interaction. The nonlocal one-body DM of the α particle was treated exactly and that of the ^{90}Zr target was treated in the CB1 approximation. The corresponding OM parameters are given in Table VI.

tion cross section σ_R in agreement with the latest experimental trend [51], although σ_R was never used as a fit parameter in the OM calculation.

$\alpha+{}^{90}$Zr system

Among medium-mass targets, ^{90}Zr has been proven to be strongly refractive for elastic α scattering, and the available elastic $\alpha+{}^{90}$Zr data were used in the past to test the $\alpha+{}^{90}$Zr optical potential [12,14,16]. In this work we have selected the elastic $\alpha+{}^{90}$Zr scattering data at $E_{\rm lab}=79.5$,99.5,118 MeV [52] and 141.7 MeV [7]. These data present a unique picture of how the refractive pattern evolves with energy. While the far-side scattering begins to dominate the large-angle scattering already at the α-particle energy of 60 MeV, the most pronounced rainbow maxima are seen as the energy reaches 80 MeV and higher [14,52].

Our folding test of the α density gave similar results as found in the $\alpha+{}^{16}$O and $\alpha+{}^{58}$Ni cases. Version A of the α density gives unrealistic oscillating pattern in the elastic cross section at large angles shown in Fig. 12, especially, at energies of around 100 MeV. The failure of version A is further confirmed by much larger χ^2 values of the OM fits to all data sets (see Table VI). Compared to the folding results obtained for these cases using the CDM3Y6 interaction and CB2 local approximation [16], the folding potentials obtained with the same interaction and densities, but using the more correct CB1 local approximation, give about the same OM fit to the data. However, the use of the CB1 approximation reduces the best-fit N_V values to around 1.08 compared to about 1.2 obtained earlier with the CB2 approximation (see Table II of Ref. [16] and Table VI). Thus the observed 20–30 % deviation from unity of the optimum N_V values in the folding analyses of elastic α-nucleus scattering [12,14,16,50] is reduced to about 10% by using a more accurate local approximation in the calculation of the exchange potential.

Finally, we want to address the approximation used for the overlap density in the folding calculation. Let us recall that the folding model generates the first order term of the Feshbach optical potential [2] which is used to obtain solution for the relative-motion wave function of the two nuclei being in their ground states. This may be only a small component of the total wave function, but it is the portion that describes the elastic scattering. With the antisymmetrization of the dinuclear system (3) properly taken into account, a reasonable approximation for the total density ρ of the two overlapping nuclei is the sum of the two densities (20). This assumption, sometimes dubbed as frozen density approximation (FDA), is widely used in the folding calculations with density dependent *NN* interaction [1,3,12,16,18]. Any density rearrangement that might happen during the collision would lead to the nuclear states different from the ground states, and thus contribute to higher order terms in the

TABLE VI. Optical potential parameters [see Eqs. (22) and (23)] used in the folding analysis of the elastic $\alpha+{}^{90}$Zr data at $E_{\rm lab}=79.5$, 99.5, 118, and 141.7 MeV. The folding potentials were obtained with three versions of the α density and Fermi form for the ^{90}Zr density (Tables I and II), using the density dependent CDM3Y6 interaction. The nonlocality of the DM was treated exactly for α and in the CB1 local approximation for ^{90}Zr. χ^2 values are per datum, and were obtained with experimental errors.

$E_{\rm lab}$ (MeV)	α dens.	N_V	$\langle r^2\rangle_V^{1/2}$ (fm)	J_V (MeV fm^3)	W (MeV)	R_W (fm)	a_W (fm)	σ_R (mb)	χ^2
79.5	A	0.958	5.130	323.6	18.48	7.175	0.531	1952	16.5
	B	1.024	5.082	314.5	18.69	7.026	0.574	1936	5.0
	C	1.083	5.062	310.2	18.98	6.943	0.601	1934	5.0
99.5	A	0.941	5.130	305.0	19.45	7.151	0.525	1963	36.3
	B	1.024	5.082	302.1	19.22	7.043	0.574	1966	9.3
	C	1.087	5.062	299.1	19.62	6.968	0.600	1968	6.3
118	A	0.930	5.131	290.6	19.02	7.024	0.650	2057	14.1
	B	1.006	5.083	286.1	19.53	6.951	0.642	2017	3.7
	C	1.069	5.063	283.6	19.99	6.897	0.649	2006	2.3
141.7	A	0.914	5.131	272.6	20.06	6.859	0.723	2088	35.3
	B	0.994	5.083	269.8	20.83	6.778	0.706	2038	9.0
	C	1.060	5.064	268.2	21.29	6.732	0.706	2022	4.1

Feshbach optical potential [2]. These higher order terms represent the ''dynamic polarization potential'' (DPP) which is energy dependent, nonlocal, and complex. The imaginary part of the DPP is the source of the imaginary part of the HI optical potential. The real part of the DPP is about an order of magnitude smaller than the folding potential [3] and that is the reason why a slightly renormalized folding potential is already a good approximation for the real part of the optical potential.

In addition to the FDA, some other approaches like the geometric or arithmetic averages of the two local densities were used for the overlap density in the folding calculation [53]. Since the effect caused by different treatments of the overlap density in the folding model has never been studied carefully, it is of interest to test different approaches in the present folding analysis. The authors of Ref. [53] have used the so-called JLM density dependent interaction [54] which was defined only for the NM density $\rho\leqslant\rho_0$, where ρ_0 is the normal nuclear matter density. To prevent the overlap density of the two nuclei from becoming significantly larger than ρ_0, so that the use of JLM parameters is appropriate, one has assumed in Ref. [53] the following arithmetic average of the two densities:

$$\rho=\frac{1}{2}\left[\rho_a\left(\boldsymbol{r}_a+\frac{\boldsymbol{s}}{2}\right)+\rho_A\left(\boldsymbol{r}_A-\frac{\boldsymbol{s}}{2}\right)\right]. \tag{24}$$

Equation (24) is denoted further in our discussion as average density approximation (ADA). It is easy to see from Eqs. (20) and (24) that the only difference between the two approaches is the factor 1/2 in front of the summed density. We show here that the ADA, which halves the overlap density at all radii, cannot account properly for the reduction in the strength of the attractive interaction that occurs as the overlap density increases. This can be seen, for example, in the radial shape of the (CDM3Y6) folding potentials for the $\alpha+{}^{90}$Zr system at $E_{\rm lab}=99.5$ MeV plotted in Fig. 13. Since the ADA gives a twice less overlap density compare to the FDA, the folding potential calculated using the ADA is more attractive and significantly deeper than that given by the FDA. This difference is much larger than that caused by using different α densities. The results for the $\alpha+{}^{90}$Zr system, using the folding potentials obtained with the ADA and FDA, are shown in Fig. 14. One can see that the excessive depth of the folding potential obtained with the ADA leads

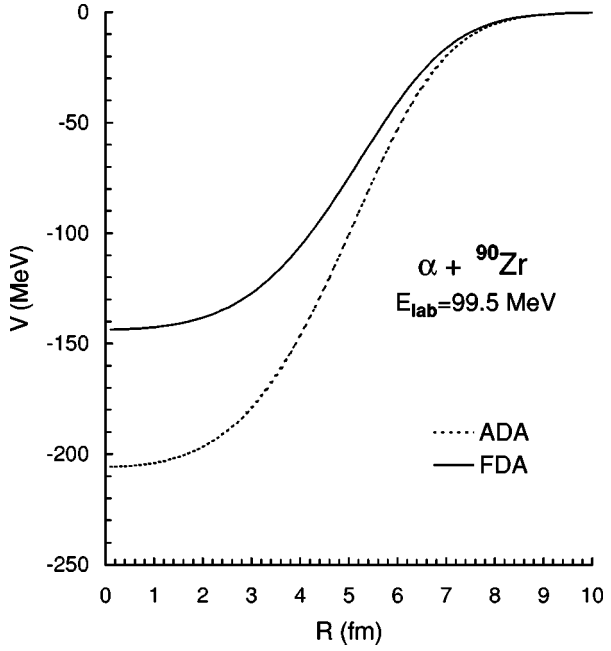

FIG. 13. Radial shape of the folding potentials for the $\alpha+{}^{90}$Zr system at $E_{\rm lab}=99.5$ MeV obtained with the h.o. model for the α density and Fermi form for the ^{90}Zr density, using average density approximation (dotted curve) and frozen density approximation (solid curve).

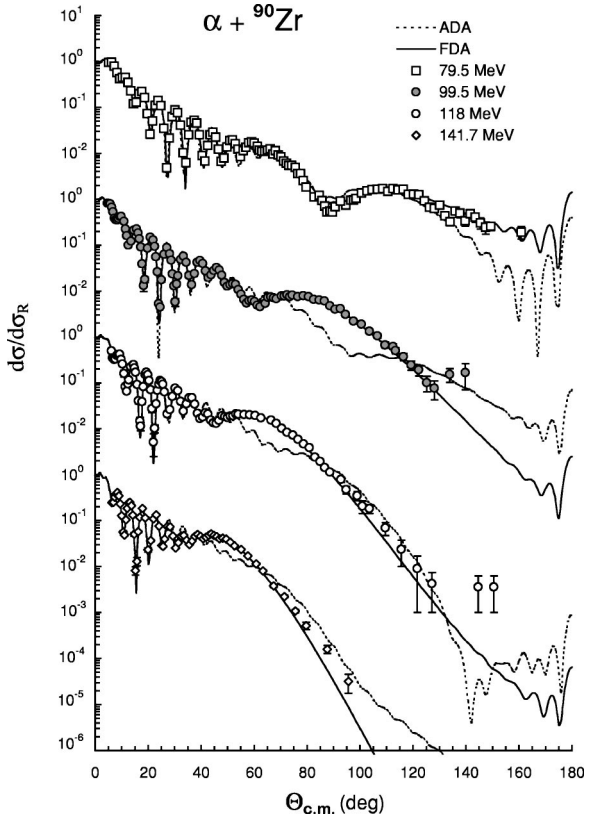

FIG. 14. Elastic $\alpha+{}^{90}$Zr scattering data at $E_{\rm lab}=79.5$, 99.5, 118, and 141.7 MeV in comparison with the OM fits given by the (CDM3Y6) folding potentials obtained with two different approximations for the overlap density: average density approximation (dotted curves) and frozen density approximation (solid curves). Version C of the α density and Fermi form for the ^{90}Zr density were used in the folding calculation.

to a complete failure in the description of data points at large angles. This effect is so strong that there was no need to perform a ''restricted'' OM analysis to figure out which approximation is better for the overlap density. We note that the strongly refractive $\alpha+{}^{90}$Zr data are the best among the studied data to test the two approaches for the overlap density.

We also stress in this connection the usefulness of the very high and compact density profile of the α particle. One has a density as high as $\rho\simeq 2\rho_0$ in the center of the ^{4}He nucleus, given by version C (see Fig. 7) or by the empirical matter density (twice the experimental charge density for ^{4}He [55] with the finite-sized charge distribution of the proton unfolded). This means that the total density for an α particle overlapping a target nucleus may reach as much as $3\rho_0$ in the FDA. See, for example, Fig. 4 of Ref. [16] where the overlap density in the $\alpha+{}^{40}$Ca system begins to approach $3\rho_0$ already at a separation of $R=4$ fm. The real optical potential can be very well determined at such a radius if the bombarding energy is sufficiently high. An artificial 50% reduction of the overlap density in the ADA leads clearly to a wrong shape of the folding potential at small distances.

V. SUMMARY

The double-folding model for the α-nucleus optical potential is revised to study the exchange effects and density dependence of the effective *NN* interaction. For this purpose, the refractive, elastic data of α scattering on ^{12}C, ^{16}O, ^{58}Ni, and ^{90}Zr targets have been analyzed within the optical model using the folding potential.

The local approximation for the nuclear density matrix in the calculation of the exchange potential was tested in the $\alpha+{}^{12}$C and $\alpha+{}^{16}$O cases by using the harmonic oscillator representation of the nonlocal DM's of the α particle and target. The most accurate version (CB1) of the Campi-Bouyssy local approximation was shown to have the numerical accuracy around 1%. The use of the CB1 approximation also reduces the best-fit renormalization factor N_V for the α-nucleus folded potential by about 15% (closer to unity) compared to that obtained earlier using the CB2 or ZE approximation.

The inclusion of a realistic density dependence into the M3Y interaction, necessary for the correct description of nuclear matter saturation properties [14], is also vital for a correct description of the refractive α-nucleus scattering data. The effect due to the presence of the DD in the effective *NN* interaction is much stronger than that caused by using different local approximations for the nuclear DM in the calculation of the exchange potential.

A high sensitivity of the refractive, elastic α-nucleus scattering data to the real optical potential at small distances enabled us to test various models for the α and target densities in the folding analysis, as well as to choose the most appropriate approximation for the overlap density in the double-folding calculation using a density dependent *NN* interaction.

Our results emphasize again the importance of the α-nucleus scattering in the nuclear structure study. The folding parameters obtained here for targets in different mass regions should also be a helpful guide in the prediction of the α-nucleus optical potential for a study of elastic scattering of loosely bound nuclei on α target using radioactive beams.

Finally, the folding formalism presented here could also provide an accurate reference potential for the local α-core interaction in the description of α-cluster structure in light and medium-mass nuclei [56].

ACKNOWLEDGMENTS

The author thanks Ray Satchler, Wolfram von Oertzen, Anders Ingemarsson, and Victor Soubbotin for their helpful communications. The research was supported, in part, by the ''Excellence'' Program of Vietnam Atomic Energy Commission (VAEC).

[1] G. R. Satchler and W. G. Love, Phys. Rep. **55**, 183 (1979).
[2] H. Feshbach, *Theoretical Nuclear Physics*, Vol. II (Wiley, New York, 1992).
[3] M. E. Brandan and G. R. Satchler, Phys. Rep. **285**, 143 (1997).
[4] G. Bertsch, J. Borysowicz, H. McManus, and W. G. Love, Nucl. Phys. **A284**, 399 (1977).
[5] N. Anantaraman, H. Toki, and G. F. Bertsch, Nucl. Phys. **A398**, 269 (1983).
[6] D. A. Goldberg, S. M. Smith, H. G. Pugh, P. G. Roos, and N. S. Wall, Phys. Rev. C **7**, 1938 (1973).
[7] D. A. Goldberg, S. M. Smith, and G. F. Burdzik, Phys. Rev. C **10**, 1362 (1974).
[8] H. G. Bohlen, M. R. Clover, G. Ingold, H. Lettau, and W. von Oertzen, Z. Phys. A **308**, 121 (1982).
[9] H. G. Bohlen, X. S. Chen, J. G. Cramer, P. Fröbrich, B. Gebauer, H. Lettau, A. Miczaika, W. von Oertzen, R. Ulrich, and Th. Wilpert, Z. Phys. A **322**, 241 (1985).
[10] E. Stiliaris, H. G. Bohlen, P. Fröbrich, B. Gebauer, D. Kolbert, W. von Oertzen, M. Wilpert, and Th. Wilpert, Phys. Lett. B **223**, 291 (1989).
[11] A. A. Ogloblin, Dao T. Khoa, Y. Kondō, Yu. A. Glukhov, A. S. Dem'yanova, M. V. Rozhkov, G. R. Satchler, and S. A. Goncharov, Phys. Rev. C **57**, 1797 (1998).
[12] A. M. Kobos, B. A. Brown, P. E. Hodgson, G. R. Satchler, and A. Budzanowski, Nucl. Phys. **A384**, 65 (1982); A. M. Kobos, B. A. Brown, R. Lindsay, and G. R. Satchler, *ibid.* **A425**, 205 (1984).
[13] Dao T. Khoa and W. von Oertzen, Phys. Lett. B **304**, 8 (1993).
[14] Dao T. Khoa and W. von Oertzen, Phys. Lett. B **342**, 6 (1995).
[15] H. A. Bethe, Annu. Rev. Nucl. Sci. **21**, 93 (1971); W. D. Myers, Nucl. Phys. **A204**, 465 (1973).
[16] Dao T. Khoa, G. R. Satchler, and W. von Oertzen, Phys. Rev. C **56**, 954 (1997).
[17] Dao T. Khoa, W. von Oertzen, H. G. Bohlen, G. Bartnitzky, H. Clement, Y. Sugiyama, B. Gebauer, A. N. Ostrowski, Th. Wilpert, M. Wilpert, and C. Langner, Phys. Rev. Lett. **74**, 34 (1995).
[18] Dao T. Khoa, W. von Oertzen, and H. G. Bohlen, Phys. Rev. C **49**, 1652 (1994).
[19] Dao T. Khoa and G. R. Satchler, Nucl. Phys. **A668**, 3 (2000).
[20] B. Sinha, Phys. Rep. **20**, 1 (1975).
[21] B. Sinha and S. A. Moszkowski, Phys. Lett. **81B**, 289 (1979).
[22] M. Ismail, M. M. Osman, and F. Salah, Phys. Lett. B **378**, 40 (1996); Phys. Rev. C **60**, 037603 (1999).
[23] V. B. Soubbotin and X. Viñas, J. Phys. G **25**, 2087 (1999); Nucl. Phys. **A665**, 291 (2000).
[24] X. Campi and A. Bouyssy, Phys. Lett. **73B**, 263 (1978).
[25] P. Ring and P. Schuck, *The Nuclear Many-Body Problem* (Springer-Verlag, New York, 1980), p. 542.
[26] R. Baltin, Z. Naturforsch. A **27A**, 1176 (1972).
[27] M. F. Vineyard, J. Cook, K. W. Kemper, and M .N. Stephens, Phys. Rev. C **30**, 916 (1984).
[28] M. El-Azab Farid and G. R. Satchler, Nucl. Phys. **A438**, 525 (1985).
[29] G. R. Satchler, Nucl. Phys. **A329**, 233 (1979).
[30] Dao T. Khoa, G. R. Satchler, and W. von Oertzen, Phys. Rev. C **51**, 2069 (1995).
[31] W. G. Love and L. W. Owen, Nucl. Phys. **A239**, 74 (1975).
[32] G. R. Satchler and Dao T. Khoa, Phys. Rev. C **55**, 285 (1997).
[33] M. E. Brandan and K. W. McVoy, Phys. Rev. C **55**, 1362 (1997).
[34] M. H. Macfarlane and S. C. Pieper, Argonne National Laboratory Report No. ANL-76-11 (1978); M. Rhoades-Brown, M. H. Macfarlane, and S. C. Pieper, Phys. Rev. C **21**, 2417 (1980); **21**, 2436 (1980).
[35] M. E. Farid and G. R. Satchler, Phys. Lett. **146B**, 389 (1984).
[36] A. Ingemarsson, A. Auce, and R. Johansson, Phys. Rev. C **49**, 1609 (1994).
[37] A. A. Ogloblin, Yu. A. Glukhov, W. H. Trzaska, A. S. Dem'yanova, S. A. Goncharov, R. Julin, S. V. Khlebnikov, M. Mutterer, M. V. Rozhkov, V. P. Rudakov, G. P. Tiorin, Dao T. Khoa, and G. R. Satchler, Phys. Rev. C **62**, 044601 (2000).
[38] Dao T. Khoa, W. von Oertzen, H. G. Bohlen, and F. Nuoffer, Nucl. Phys. **A672**, 387 (2000).
[39] G. Hauser, R. Löhken, H. Rebel, G. Schatz, G. W. Schweimer, and J. Specht, Nucl. Phys. **A128**, 81 (1969).
[40] S. Wiktor, C. Mayer-Böricke, A. Kiss, M. Rogge, P. Turek, and H. Dabrowski, Acta Phys. Pol. B **12**, 491 (1981); A. Kiss, C. Mayer-Böricke, M. Rogge, P. Turek, and S. Wiktor, J. Phys. G **13**, 1067 (1987).
[41] H. De Vries, C. W. De Jager, and C. De Vries, At. Data Nucl. Data Tables **36**, 495 (1987).
[42] J. S. Al-Khalili, J. A. Tostevin, and I. J. Thompson, Phys. Rev. C **54**, 1843 (1996).
[43] O. M. Knyazkov, I. N. Kuchtina, and S. A. Fayans, Phys. Part. Nucl. **30**, 369 (1999).
[44] H. Abele, H. J. Hauser, A. Körber, W. Leitner, R. Neu, H. Plappert, T. Rohwer, G. Staudt, M. Strasser, S. Welte, M. Walz, P. D. Eversheim, and F. Hinterberger, Z. Phys. A **326**, 373 (1987).
[45] M. Frances, Ph.D. thesis, University of California, 1968.
[46] G. R. Satchler (private communication).
[47] H. H. Chang *et al.*, Nucl. Phys. **A270**, 413 (1976).
[48] H. Rebel, R. Löhken, G. W. Schweimer, G. Schatz, and G. Hauser, Z. Phys. **256**, 258 (1972).
[49] J. Albinski *et al.*, Nucl. Phys. **A445**, 477 (1985).
[50] U. Atzrott, P. Mohr, H. Abele, C. Hillenmayer, and G. Staudt, Phys. Rev. C **53**, 1336 (1996).
[51] A. Ingemarsson, J. Nyberg, P. U. Renberg, O. Sundberg, R. F. Carlson, A. J. Cox, A. Auce, R. Johansson, G. Tibell, Dao T. Khoa, and R. E. Warner, Nucl. Phys. **A676**, 3 (2000).
[52] L. W. Put and A. M. J. Paans, Nucl. Phys. **A291**, 93 (1977).
[53] L. Trache, A. Azhari, H. L. Clark, C. A. Gagliardi, Y. W. Lui, A. M. Mukhamedzhanov, R. E. Tribble, and F. Carstoiu, Phys. Rev. C **61**, 024612 (2000).
[54] J. P. Jeukenne, A. Lejeune, and C. Mahaux, Phys. Rev. C **16**, 80 (1977).
[55] I. Sick, J. S. McCarthy, and R. R. Whitney, Phys. Lett. **64B**, 33 (1976).
[56] F. Michel, S. Ohkubo, and G. Reidermeister, Prog. Theor. Phys. Suppl. **132**, 7 (1998); T. Sakuda and S. Ohkubo, *ibid.* **132**, 103 (1998).